

# Geophysical Research Letters®

## RESEARCH LETTER

10.1029/2022GL102594

### Key Points:

- An imbalance between input and removal produces an ~3-fold seasonal increase in the euphotic-zone inventory of dissolved iron (DFe) near Bermuda
- Analyses of iron in seasonal-scale aerosols, rain and water-column samples allow direct estimates of the replacement time of DFe
- We derive a mean residence time of ~0.8–1.9 years for DFe in the euphotic zone (<200 m) of the Sargasso Sea near Bermuda

### Supporting Information:

Supporting Information may be found in the online version of this article.

### Correspondence to:

P. N. Sedwick,  
psedwick@odu.edu

### Citation:

Sedwick, P. N., Sohst, B. M., Buck, K. N., Caprara, S., Johnson, R. J., Ohnemus, D. C., et al. (2023). Atmospheric input and seasonal inventory of dissolved iron in the Sargasso Sea: Implications for iron dynamics in surface waters of the subtropical ocean. *Geophysical Research Letters*, 50, e2022GL102594. <https://doi.org/10.1029/2022GL102594>

Received 3 JAN 2023

Accepted 3 MAR 2023

© 2023. The Authors.

This is an open access article under the terms of the Creative Commons Attribution-NonCommercial-NoDerivs License, which permits use and distribution in any medium, provided the original work is properly cited, the use is non-commercial and no modifications or adaptations are made.

## Atmospheric Input and Seasonal Inventory of Dissolved Iron in the Sargasso Sea: Implications for Iron Dynamics in Surface Waters of the Subtropical Ocean

P. N. Sedwick<sup>1</sup> , B. M. Sohst<sup>1</sup> , K. N. Buck<sup>2,3</sup>, S. Caprara<sup>2</sup>, R. J. Johnson<sup>4</sup> , D. C. Ohnemus<sup>5</sup> , L. E. Sofen<sup>6</sup> , A. Tagliabue<sup>7</sup> , B. S. Twining<sup>6</sup> , and T. E. Williams<sup>1</sup> 

<sup>1</sup>Department of Ocean and Earth Sciences, Old Dominion University, Norfolk, VA, USA, <sup>2</sup>College of Marine Science, University of South Florida, St. Petersburg, FL, USA, <sup>3</sup>College of Earth, Ocean, and Atmospheric Sciences, Oregon State University, Corvallis, OR, USA, <sup>4</sup>Bermuda Institute of Ocean Sciences, St. Georges, Bermuda, <sup>5</sup>Skidaway Institute of Oceanography, University of Georgia, Savannah, GA, USA, <sup>6</sup>Bigelow Laboratory for Ocean Sciences, East Boothbay, ME, USA, <sup>7</sup>School of Environmental Sciences, University of Liverpool, Liverpool, UK

**Abstract** Constraining the role of dust deposition in regulating the concentration of the essential micronutrient iron in surface ocean waters requires knowledge of the flux of seawater-soluble iron in aerosols and the replacement time of dissolved iron (DFe) in the euphotic zone. Here we estimate these quantities using seasonally resolved DFe data from the Bermuda Atlantic Time-series Study region and weekly-scale measurements of iron in aerosols and rain from Bermuda during 2019. In response to seasonal changes in vertical mixing, primary production and dust deposition, surface DFe concentrations vary from ~0.2 nM in early spring to >1 nM in late summer, with DFe inventories ranging from ~30 to ~80  $\mu\text{mol}/\text{m}^2$ , respectively, over the upper 200 m. Assuming the upper ocean approximates steady state for DFe on an annual basis, our aerosol and rainwater data require a mean euphotic-zone residence time of ~0.8–1.9 years for DFe with respect to aeolian input.

**Plain Language Summary** Primary production by phytoplankton in ocean surface waters is the foundation of the marine ecosystem, and plays a key role in maintaining the ocean-atmosphere balance of carbon dioxide, which regulates global climate. Iron is an essential micronutrient that is required by phytoplankton, and the availability of dissolved iron (DFe) is thought to limit phytoplankton growth over large areas of the ocean. In this context, it is important to constrain the sources and persistence of DFe in surface ocean waters, which control the amount of DFe that is available to support phytoplankton growth. This study focuses on the Bermuda region of the North Atlantic Ocean, where deposition of airborne soil dust is the major source of DFe to surface waters. By combining measurements of the atmospheric loading and solubility of iron in soil dust over Bermuda with measurements of DFe in adjacent ocean waters over a full year, we are able to estimate the rate of supply of DFe from dust deposition in this region, as well as the average time that this DFe persists in the surface ocean. The latter, termed the DFe replacement time, is around 1 year, which agrees well with recent estimates from comparable ocean regions.

## 1. Introduction

Iron is an essential micronutrient for marine phytoplankton, and dissolved iron (DFe) supply regulates primary production and nitrogen fixation over large areas of the surface ocean (Boyd & Ellwood, 2010; Kustka et al., 2002; Martin et al., 1991; Moore et al., 2013; Wen et al., 2022). A primary source of DFe to open-ocean surface waters is deposition and partial dissolution of mineral aerosols (dust), and considerable effort has been directed at quantifying the air-to-sea fluxes and seawater solubility of aerosol iron (Hamilton et al., 2022; Jickells et al., 2005; Mahowald et al., 2018; Sholkovitz et al., 2012; Tagliabue et al., 2017). Recent work has also focused on estimating the replacement time of DFe in surface ocean waters with respect to the aeolian input; that is, the surface-ocean inventory of DFe divided by the atmospheric input of seawater-soluble iron. If calculated over timescales for which a system approaches steady state, and assuming atmospheric input is the major DFe source, then this replacement time is equivalent to the residence time of DFe in the surface ocean (Black et al., 2020; Hayes et al., 2015, 2018; Kadko et al., 2019). Importantly, the replacement time of DFe modulates the concentration of this micronutrient in the euphotic zone, and thus the propensity for iron availability to regulate primary

production in ocean ecosystems. Moreover, empirical estimates of DFe replacement time provide a robust constraint on the veracity of numerical models of the ocean iron cycle (Tagliabue et al., 2016).

One strategy for deriving such information is to combine estimates of atmospheric deposition of iron and other input fluxes with water-column inventories of DFe and other tracers in specific oceanic locations, which has yielded surface-ocean DFe replacement times ranging from months to decades (e.g., Boyle et al., 2005; Croot et al., 2004; Hayes et al., 2015; Jickells, 1999; Kadko et al., 2019; Ussher et al., 2013). However, these studies have thus far lacked direct estimates of soluble iron deposition over periods comparable to the replacement time of DFe, which should provide a stronger constraint on the relationship between aeolian input and water-column inventory. We apply this approach using seasonally resolved measurements of DFe in water column samples collected from the Bermuda Atlantic Time-series Study (BATS) region during 2019 along with measurements of iron in aerosols and rainwater collected on Bermuda over the same time period, to probe the dynamics of DFe in the western subtropical North Atlantic Ocean (Sargasso Sea). Our data reveal substantial seasonal variations in the DFe inventory of the euphotic zone, consistent with previously reported data from this ocean region (Hatta et al., 2015; Middag et al., 2015; Sedwick et al., 2005, 2020; Wu & Boyle, 2002), indicating that the system is not in steady state over sub-annual timescales. However, those data also reveal that the seasonal progression of DFe concentrations in surface waters of the BATS region is relatively consistent, implying that the upper-ocean DFe inventory is close to steady state from year to year. If so, then our data can be used to estimate an “annualized-average” replacement time, or mean residence time, for DFe in the upper water column of the BATS region. Our results agree with several recent studies that have estimated a replacement time on the order of 1 year for DFe in surface waters of the subtropical oceans.

## 2. Methods

### 2.1. Collection and Processing of Water-Column Samples

As part of the Bermuda Atlantic Iron Time-series (BAIT) project, GEOTRACES Process Study GApr13, water-column samples for trace metal measurements were collected from the BATS site (31°40'N, 64°10'W) and adjacent BATS spatial stations (Figure 1) during cruises in March (spring), May (early summer), August (late summer) and November (fall) 2019 aboard RV *Atlantic Explorer* and RV *Endeavor*. Seawater samples and hydrographic data were collected using a trace-metal clean conductivity-temperature-depth sensor (SBE 19 plus, SeaBird Electronics) mounted on a custom-built trace-metal clean carousel (SeaBird Electronics) fitted with custom-modified 5-L Teflon-lined external-closure Niskin-X samplers (General Oceanics) and deployed on an Amsteel non-metallic line (Sedwick et al., 2022). On the August cruise, we also collected near-surface samples (~1 m depth) in a Niskin-X sampler deployed from an inflatable dinghy ~500 m upwind of the research vessel, to avoid contamination from the ship. After recovery, the seawater samples were filtered through pre-cleaned 0.2-μm pore AcroPak Supor filter capsules (Pall) using filtered nitrogen gas inside a shipboard clean laboratory (Sedwick et al., 2020, 2022). For DFe analysis, filtrate was collected in acid-cleaned 125 mL low-density polyethylene (LDPE) bottles (Nalgene) and acidified to pH 1.7 post-cruise by addition of 6 M ultrapure hydrochloric acid (Fisher Optima).

### 2.2. Collection and Processing of Aerosol and Rain Samples

As part of the BAIT project, we also collected composite samples of bulk aerosol and rainwater atop the 23-m height sampling tower at Tudor Hill, Bermuda (32°15.9'N 64°52.6'W, Figure 1), on an approximately weekly basis from November 2018 through March 2020, bracketing the four project cruises. Aerosols were collected with a high-volume sampler on acid-cleaned Whatman-41 cellulose filters (20 μm nominal pore size), which collect particles as small as 1 μm with >90% efficiency (e.g., Stafford & Ettinger, 1972). The coastal Tudor Hill site faces into the prevailing southwesterly winds (Sorooshian et al., 2020), so aerosols were only collected during winds >1 m s<sup>-1</sup> from 210° to 315° in order to avoid local sources. Sample filters were stored in zip-lock polyethylene bags in a vacuum desiccator. For analysis of “total aerosol iron”, portions of the aerosol sample filters were digested with a mixture of ultrapure concentrated nitric and hydrofluoric acids and hydrogen peroxide (Fisher Optima) in Teflon vessels (Morton et al., 2013), using a microwave heating system (CEM MARS 6), then evaporated on a hot plate and diluted to volume with 2% (v/v) ultrapure nitric acid. Replicate portions of the aerosol filters were also subjected to a flow-through leaching procedure modified from Buck et al. (2006) using 250 mL of high-purity deionized water (DIW, Barnstead Nanopure, >18.2 MΩ-cm resistivity), and the leachate

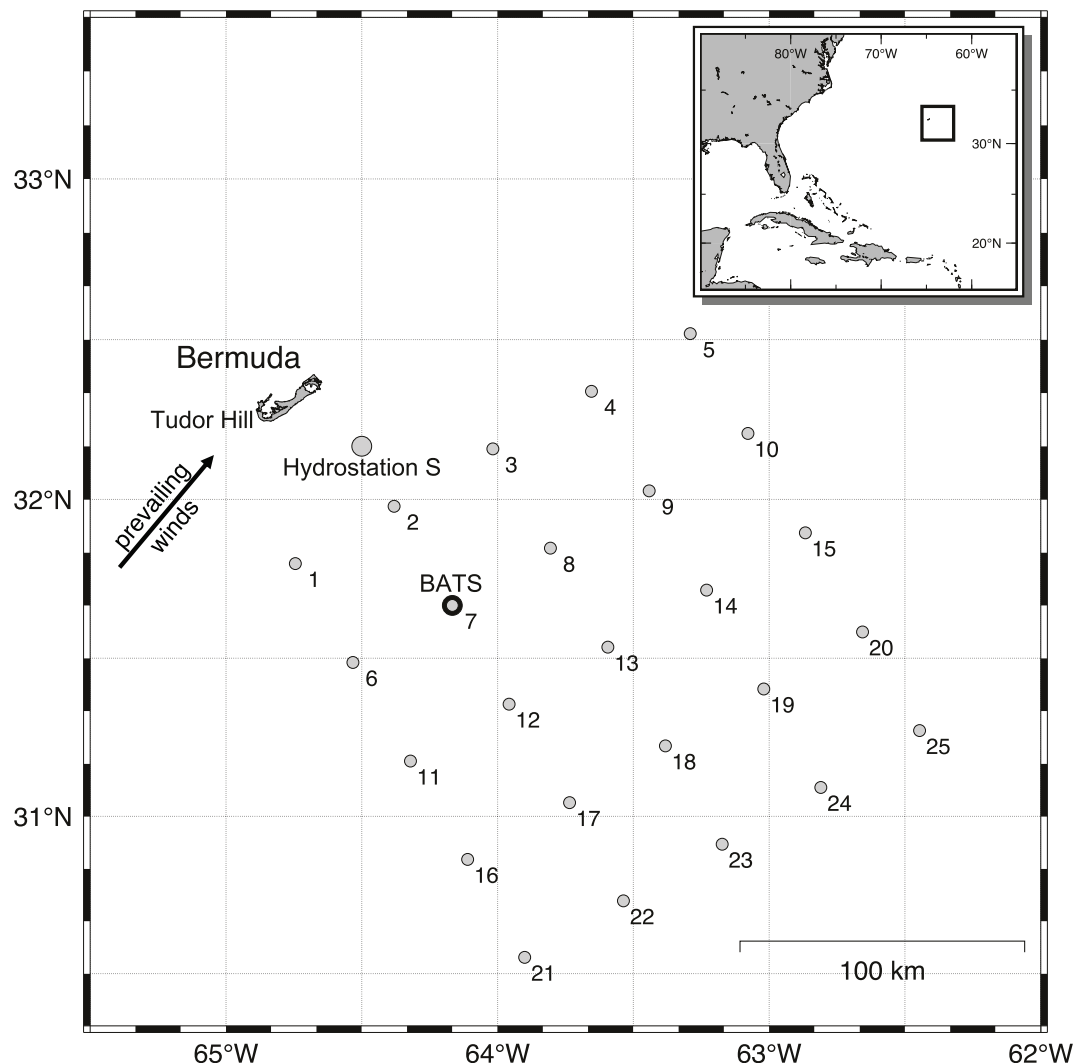


**Figure 1.** Study region showing locations of Bermuda Atlantic Time-series Study (BATS) site (station 7) and adjacent BATS spatial stations where water-column samples were collected, and Tudor Hill on Bermuda where aerosols and rainwater were collected (map courtesy of Paul Lethaby).

acidified to 0.4% (v/v) with 6 M ultrapure hydrochloric acid (Fisher Optima) for analysis of “DIW-soluble aerosol iron” ( $\text{Fe}_{\text{S-DIW}}$ ); the same filter portions were then subjected to a batch leach procedure modified from Kadko et al. (2019) using 25% acetic acid (HOAc, Fisher Optima) and 0.02 M hydroxylamine hydrochloride (Sigma) at 90°C, and the supernatant leachate evaporated and then diluted in 2% ultrapure nitric acid (Fisher Optima) for analysis of “HOAc-soluble aerosol iron” ( $\text{Fe}_{\text{S-HOAc}}$ ). Rainwater samples were collected in acid-cleaned 2-L wide-mouth fluorinated high density polyethylene bottles (Nalgene) using an automatic rain sampler (N-Con Systems ADS 00–120); the rain samples were subsequently acidified to 0.4% (v/v) with 6 M ultrapure hydrochloric acid (Fisher Optima) in these bottles, and then after 2 months the acidified, unfiltered samples were transferred into acid-cleaned 125 mL LDPE bottles (Nalgene) for analysis of “total-dissolvable Fe” (TDFe; Sedwick et al., 2007). Field blanks for the aerosols (an acid-cleaned filter) and rainwater (125 mL ultrapure DIW) were deployed on the Tudor Hill tower and processed in the same manner as samples, but without operating or opening the aerosol or rain samplers, respectively.

### 2.3. Iron Measurements in Water-Column, Aerosol and Rain Samples

Dissolved iron was determined in water-column samples using inductively-coupled plasma mass spectrometry (ICP-MS, Thermo Fisher Scientific ElementXR) with in-line separation-preconcentration (Elemental Scientific

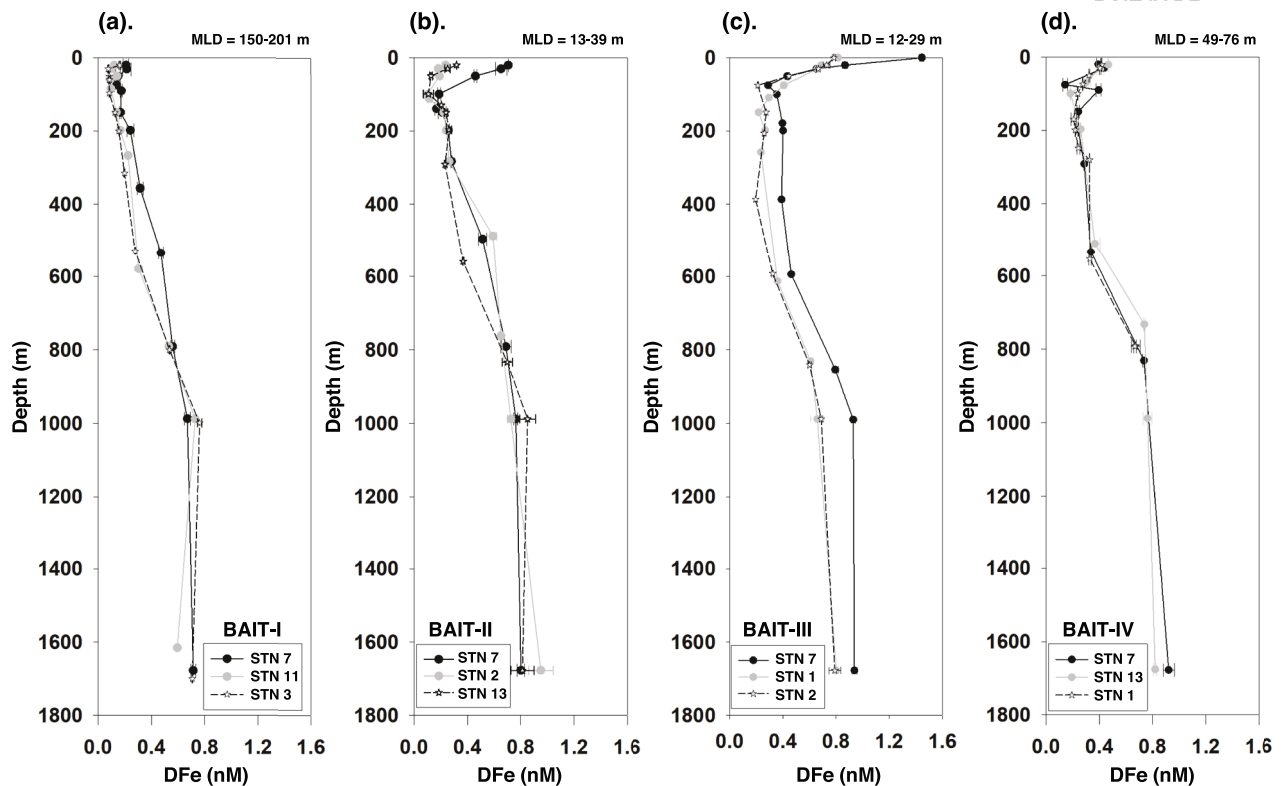


**Figure 2.** Dissolved iron (DFe) concentration profiles from BATS spatial stations (see Figure 1) during BAIT project cruises in (a). March 2019 (BAIT-I), (b). May 2019 (BAIT-II), (c). August 2019 (BAIT-III), and (d). November 2019 (BAIT-IV). Mixed layer depths (MLD) shown at top.

SeaFAST SP3) modified after Lagerström et al. (2013). Analytical precision is estimated at better than  $\pm 10\%$  (one sigma) for DFe  $> 0.2$  nM, with a limit of detection estimated at 0.05 nM. Iron was determined in aerosol digest solutions, aerosol leachate solutions and acidified rainwater by ICP-MS without preconcentration, with analytical precision estimated at better than  $\pm 25\%$  (one sigma) for total aerosol iron, TDFe in rain, and soluble iron in aerosols and rain. Estimated limits of detection were 0.159, 0.011, and 0.011  $\mu\text{mol}$  per filter, for total aerosol iron, DIW-soluble aerosol iron and HOAc-soluble aerosol iron, respectively, and 0.002 nmol per sample for TDFe in rainwater. Further details of the analytical methods are provided in Supporting Information S1.

### 3. Results and Discussion

#### 3.1. Seasonal Changes in DFe Inventory of the Upper Water Column

The BATS site is located at the northwestern extent of the North Atlantic Subtropical Gyre, and is subject to deep convective mixing that ranges from 100 to 400 m, which commences in the late fall and continues through early spring, when biological production is typically highest (Lomas et al., 2013). The upper water column then warms and stratifies during the spring, resulting in a shallow ( $< 50$  m), oligotrophic surface mixed layer during summer (Lomas et al., 2013; Steinberg et al., 2001; Tin et al., 2016). This and the elevated deposition of North African mineral aerosols during the summer months (Jickells, 1999; Prospero et al., 2002) results in a pronounced seasonal variation of DFe in the upper water column: biological uptake and scavenging result in uniformly low concentrations in winter-early spring, after which aeolian DFe accumulates from spring through late summer as the mixed layer shoals, then concentrations decrease in the fall as convective mixing commences (Sedwick et al., 2005, 2020; Wu & Boyle, 2002).

This seasonal pattern is evident in the DFe data from our four BAIT cruises (Figure 2), with surface concentrations ranging from  $\sim 0.1$ – $0.2$  nM in March to  $\sim 0.7$ – $1.5$  nM in August, as mixed layer depths shallowed from  $\sim 150$ – $200$  m to  $\sim 10$ – $30$  m. These seasonal changes correspond to a nearly three-fold variation in the DFe

**Table 1***Estimated Dissolved Iron (DFe) Inventories Over the Upper 200 m of the Water Column During the Bermuda Atlantic Iron Time-Series Cruises in 2019*

Cruise	BAIT-I	BAIT-II	BAIT-III	BAIT-IV	Overall mean
DFe inventory ( $\mu\text{mol m}^{-2}$ )	$28.1 \pm 7.4$	$48.9 \pm 17.5$	$84.1 \pm 11.7$	$55.4 \pm 2.1$	$54.1 \pm 23.0$

*Note.* Values represent mean  $\pm$  one standard deviation of estimates for the three vertical DFe concentration profiles for each cruise (see Figure 2).

inventory of the upper water column (Table 1), which for the purpose of this study we define as the upper 200 m (the maximum mixed layer depth observed during our four cruises), encompassing the depth range of the euphotic zone in the BATS region (e.g., Siegel et al., 1995). Our inventory estimates indicate that DFe is clearly not at steady state in the upper water column of the Sargasso Sea over seasonal timescales: input exceeds removal during the spring through late summer, whereas removal exceeds input during the fall through early spring. Nevertheless, water-column DFe data from the BATS region in preceding years (Hatta et al., 2015; Middag et al., 2015; Sedwick et al., 2005, 2015, 2020) reveal near-surface concentrations consistent with our BAIT data for early spring ( $\sim 0.2$  nM), late summer ( $\sim 1$  nM), and fall ( $\sim 0.5$  nM), suggesting that the upper ocean does approximate steady state with respect to DFe inventory over annual timescales. With that assumption, estimates of the deposition of soluble aerosol iron over that same period, as described in Section 3.2, may be used to calculate an annualized average replacement time for DFe in the upper water column of the BATS region.

### 3.2. Estimating Dry and Wet Deposition of Soluble Iron

Analyses of the bulk aerosols and rainwater collected on Bermuda allow estimates of the dry and wet deposition of soluble iron during each sampling interval. We calculate dry deposition of soluble aerosol iron from the atmospheric loading of either  $\text{Fe}_{\text{S-DIW}}$  or  $\text{Fe}_{\text{S-DIW}} + \text{Fe}_{\text{S-HOAc}}$ , which likely bracket the proportion of total aerosol iron that is released as DFe in surface seawater (Ito et al., 2019; Shelley et al., 2018), multiplied by the aerosol deposition velocity and the duration of the sampling period. For deposition velocity we assume a value of  $1 \text{ cm s}^{-1}$ , which is near the mean of values estimated for Bermuda (Arimoto et al., 2003; Kadko et al., 2020; Tian et al., 2008), as further discussed in Section 3.3. Wet deposition of soluble aerosol iron during each sampling period is estimated from the product of the TDFe concentration of rainwater, the corresponding rainfall amount, and the fractional solubility of aerosol iron during the sampling period calculated using either  $\text{Fe}_{\text{S-DIW}}$  or  $\text{Fe}_{\text{S-DIW}} + \text{Fe}_{\text{S-HOAc}}$ . This approach is based on previous data from the Bermuda region, which indicate that the ratio of dissolved- to total-dissolvable iron (DFe/TDFe) concentration in rainwater is generally similar to the fractional solubility of iron in contemporaneously collected aerosols (Sedwick et al., 2007); this notwithstanding the fact that TDFe concentrations can be substantially less than total iron concentrations in rainwater (Kim & Church, 2001; Tian et al., 2008). The thus estimated deposition of soluble iron for sampling periods from November 2018 through March 2020 (Figure 3) suggest that dry deposition dominates overall, as reported by some previous studies (Arimoto et al., 1995; Tian et al., 2008), although wet deposition dominates in late spring and late fall.

### 3.3. Estimating Replacement Time of Dissolved Iron in the Upper Water Column

If we assume that the upper water column in the BATS region is at steady state with respect to DFe over annual timescales, then an “annualized-average” replacement time—essentially a mean residence time—can be estimated for DFe with respect to atmospheric deposition. This we calculate as the mean inventory of DFe over the upper 200 m from all sampling casts completed during the four BAIT cruises (Figure 2) divided by the annualized mean flux of soluble iron in aerosols and rain on Bermuda. The latter is calculated as the sum of dry and wet deposition of soluble iron (see Section 3.2 and Figure 3) over calendar year 2019 divided by the total duration of the aerosol sampling days during that year (318 days), noting that Hurricane Humberto and the resulting power outage interrupted sampling from 16 September through 21 October (that 5-week unsampled period is not included in our calculation of mean aeolian flux). These calculations yield mean residence times for DFe in the upper 200 m of 1.94 years if aeolian fluxes are estimated using DIW-soluble aerosol iron, or 0.80 years if aeolian fluxes estimated using DIW-soluble aerosol iron plus HOAc-soluble aerosol iron (Table 2). Implicit in these estimates is the assumption of regional coherence between atmospheric deposition on Bermuda and in the BATS region, which is supported by a previous comparison between contemporaneous aerosol samples collected from both locations (Sholkovitz & Sedwick, 2006). Our estimates also neglect aerosols deposited to the Bermuda

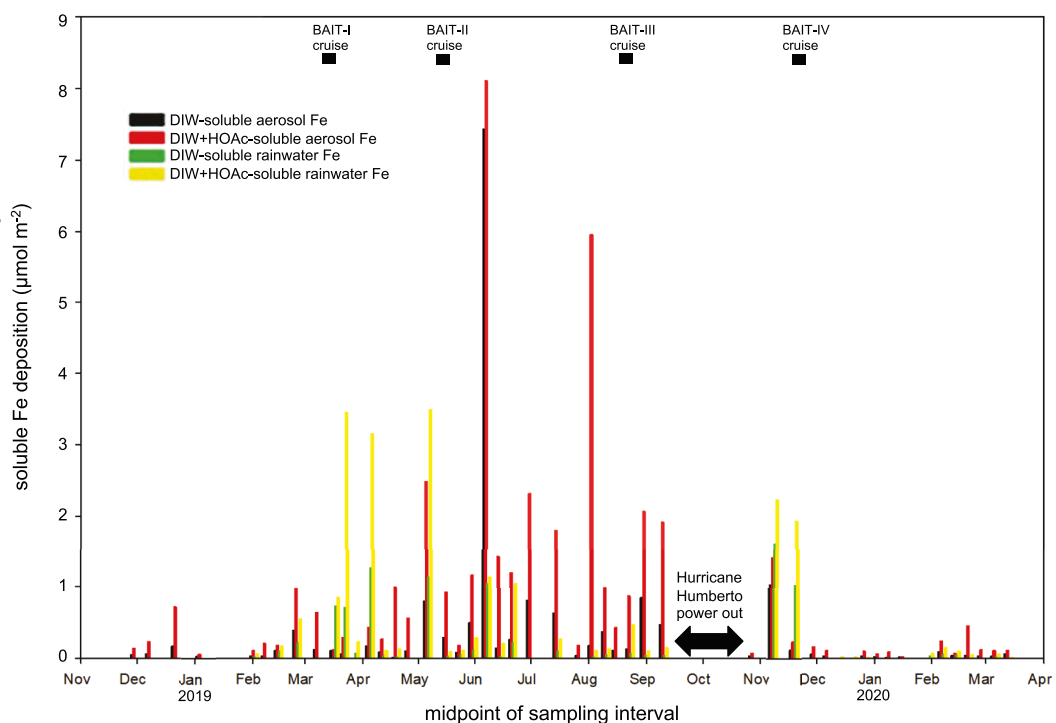


**Figure 3.** Calculated deposition of soluble iron in aerosols and rainwater for each sampling period on Bermuda, using results for both DIW-soluble aerosol iron and DIW-soluble aerosol iron plus HOAc-soluble aerosol iron. Periods of BAIT cruises and power outage are indicated.

region when winds were outside the prevailing direction of  $210^{\circ}$ – $315^{\circ}$ , which are not sampled at Tudor Hill (see Section 2.2).

As well as the estimated analytical uncertainties shown in Table 2, there are additional uncertainties in our replacement time estimates that arise from the deposition velocity of aerosol iron, and the operational definitions of the fractional solubility of iron in aerosols and rainwater. For dry deposition velocity, Arimoto et al. (2003) suggest a value of  $1 \text{ cm s}^{-1} \pm$  a factor of three for mineral dust and other supermicrometer particles not associated with sea salt, which is largely consistent with seasonally-resolved empirical estimates of  $0.1$ – $0.3 \text{ cm s}^{-1}$  in summer and  $2$ – $6 \text{ cm s}^{-1}$  in fall-winter using data from Bermuda (Tian et al., 2008). More recently, Kadko et al. (2020) describe a global relationship between bulk deposition velocities estimated using beryllium-7 and rainfall rate, which yields an aerosol dry deposition velocity of  $1.2 \text{ cm s}^{-1}$ . Given that the latter value is based on average aerosol beryllium-7 activities and monthly average rainfall rates suggests that our assumed dry deposition velocity of  $1 \text{ cm s}^{-1}$  is reasonable. Between the two leaching methods used to estimate the fractional solubility of aerosol iron, the sub-annual mean residence time of DFe calculated using the sequential DIW and HOAc leaches is most consistent with our field observations. Indeed, the increase in the water-column DFe inventory from early spring through late summer, in apparent response to the seasonal increase in aeolian iron input, implies a DFe residence time of around 6 months.

**Table 2**

Summary of Mean Replacement Time Estimate for Dissolved Iron (DFe) in the Upper Water Column

	Using DIW-soluble Fe	Using DIW + HOAc-soluble Fe
Annualized mean deposition of soluble Fe ( $\mu\text{mol m}^{-2} \text{ yr}^{-1}$ )	$27.8 \pm 7.0^{\text{a}}$	$68.0 \pm 12.3^{\text{b}}$
Mean DFe inventory over upper 200 m ( $\mu\text{mol m}^{-2}$ )	$54.1 \pm 23.0$	$54.1 \pm 23.0$
Mean replacement time for DFe in upper 200 m (yr)	$1.94 \pm 0.95^{\text{b}}$	$0.80 \pm 0.37^{\text{b}}$

<sup>a</sup>Using an estimated one-sigma analytical uncertainty of 25% (see Section 2.3). <sup>b</sup>Calculated by propagation of estimated analytical errors (Skoog et al., 2007).

It should also be noted that there is considerable variability in near-surface DFe concentrations at the submeso- to mesoscale in the Sargasso Sea during the summer (Sedwick et al., 2020), which adds uncertainty to our DFe inventory estimates, although our sampling at the BATS station (station 7 in Figure 1) as well as adjacent spatial stations during each cruise (e.g., see concentration differences in the upper 100 m in Figures 2b and 2c) likely dampens the impact of such lateral concentration gradients on the mean DFe inventories. However, it is conceivable that mesoscale eddies could provide a net source of DFe to the upper water column of the BATS region over seasonal to annual timescales (Conway et al., 2018; Sedwick et al., 2020), in which case our estimates of DFe residence time based on aeolian input only (i.e., ignoring lateral advective inputs) would constitute an overestimate. For example, Conway et al. (2018) argue that cold-core eddies may supply between 3% and 75% of the aeolian input of DFe to the upper water column of the North Atlantic Subtropical Gyre, in which case our residence times would be overestimated by as much as  $\sim$ 4–10 months, depending on the leaching method used to define seawater-soluble aerosol iron. Any vertical resupply of DFe from below the euphotic zone would also reduce our residence time estimates, although that flux is expected to be small in the BATS region, given the generally gentle vertical gradients in DFe concentration over the 200–400 m depth range (Figure 2).

#### 4. Conclusions

Our estimate of 0.8–1.9 years for the mean residence time of DFe in the upper 200 m of the BATS region is generally consistent with several recent estimates for comparable settings and depth ranges in the oligotrophic open-ocean. Focusing on aeolian input, Hayes et al. (2015, 2018) used thorium-230 and thorium-232 to estimate replacement times of 0.5–1 year for DFe in the upper 250 m at the Hawaii Ocean Time-series station ALOHA in the subtropical North Pacific, and  $<1$  year for the upper 200 m along the GEOTRACES GA03 transect, which included the BATS station. A more recent study of iron cycling at station ALOHA similarly used water-column measurements of thorium and DFe to calculate a replacement time of  $\sim$ 0.7 years for DFe in the upper 150 m (Hawco et al., 2022). Finally, Black et al. (2020) have combined a compilation of thorium-234 and sediment trap data to quantify the removal of DFe via export of biogenic and authigenic particles, from which they infer mean and median residence times of 2 and 0.12 years, respectively, for DFe in the upper 200 m of the subtropical gyres. These relatively short residence times point to the dynamic nature of DFe in the surface ocean, and thus the potential for rapid onset of iron limitation of phytoplankton growth due to seasonal imbalances between the input and removal of DFe from the euphotic zone—even in high-dust regimes such as the subtropical North Atlantic.

#### Data Availability Statement

Data presented and discussed here, and associated metadata, are available from the U.S. National Science Foundation's Biological and Chemical Oceanography Data Management Office at: <https://www.bco-dmo.org/project/822807>.

#### Acknowledgments

We gratefully acknowledge the assistance of the crews and marine technicians of RV *Atlantic Explorer* and RV *Endeavor*, the BATS program team, and Dan Dickinson, Shannon Burns, Matt Hayden and Andrew Peters. This research was supported by U.S. National Science Foundation awards 1829833 to PNS, 1829777 to KNB, 1829844 to RJ, 1829819 to BST and 1829686 to Andrew Peters, and U.K. National Environment Research Council award NE/S013547/1 to AT.

#### References

Arimoto, R., Duce, R. A., Ray, B. J., Ellis, W. G., Jr., Cullen, J. D., & Merrill, J. T. (1995). Trace elements in the atmosphere over the North Atlantic. *Journal of Geophysical Research*, 100(D1), 1199–1213. <https://doi.org/10.1029/94jd02618>

Arimoto, R., Duce, R. A., Ray, B. J., & Tomza, U. (2003). Dry deposition of trace elements to the western North Atlantic. *Global Biogeochemical Cycles*, 17(1). <https://doi.org/10.1029/2001gb001406>

Black, E. E., Kienast, S. S., Lemaitre, N., Lam, P. J., Anderson, R. F., Planquette, H., et al. (2020). Ironing out Fe residence time in the dynamic upper ocean. *Global Biogeochemical Cycles*, 34(9), e2020GB006592. <https://doi.org/10.1029/2020gb006592>

Boyd, P. W., & Ellwood, M. J. (2010). The biogeochemical cycle of iron in the ocean. *Nature Geoscience*, 3(10), 675–682. <https://doi.org/10.1038/ngeo964>

Boyle, E. A., Bergquist, B. A., Kayser, R. A., & Mahowald, N. (2005). Iron, manganese, and lead at Hawaii Ocean Time-series station ALOHA: Temporal variability and an intermediate water hydrothermal plume. *Geochimica et Cosmochimica Acta*, 69(4), 933–952. <https://doi.org/10.1016/j.gca.2004.07.034>

Buck, C. S., Landing, W. M., Resing, J. A., & Lebon, G. T. (2006). Aerosol iron and aluminum solubility in the northwest Pacific Ocean: Results from the 2002 IOC cruise. *Geochemistry, Geophysics, Geosystems*, 7(4), Q04M07. <https://doi.org/10.1029/2005gc000977>

Conway, T. M., Palter, J. B., & de Souza, G. F. (2018). Gulf Stream rings as a source of iron to the North Atlantic subtropical gyre. *Nature Geoscience*, 11(8), 594–598. <https://doi.org/10.1038/s41561-018-0162-0>

Croot, P. L., Streu, P., & Baker, A. R. (2004). Short residence time for iron in surface seawater impacted by atmospheric dry deposition from Saharan dust events. *Geophysical Research Letters*, 31(23), L23S08. <https://doi.org/10.1029/2004gl020153>

Hamilton, D. S., Perron, M. M., Bond, T. C., Bowie, A. R., Buchholz, R. R., Guieu, C., et al. (2022). Earth, wind, fire, and pollution: Aerosol nutrient sources and impacts on ocean biogeochemistry. *Annual Review of Marine Science*, 14(1), 303–330. <https://doi.org/10.1146/annurev-marine-031921-013612>

Hatta, M., Measures, C. I., Wu, J., Roshan, S., Fitzsimmons, J. N., Sedwick, P., & Morton, P. (2015). An overview of dissolved Fe and Mn distributions during the 2010–2011 US GEOTRACES North Atlantic cruises: GEOTRACES GA03. *Deep Sea Research Part II: Topical Studies in Oceanography*, 116, 117–129. <https://doi.org/10.1016/j.dsr2.2014.07.005>

Hawco, N. J., Yang, S. C., Pinedo-González, P., Black, E. E., Kenyon, J., Ferrón, S., et al. (2022). Recycling of dissolved iron in the North Pacific subtropical gyre. *Limnology & Oceanography*, 67(11), 2448–2465. <https://doi.org/10.1002/leo.12212>

Hayes, C. T., Anderson, R. F., Cheng, H., Conway, T. M., Edwards, R. L., Fleisher, M. Q., et al. (2018). Replacement times of a spectrum of elements in the North Atlantic based on thorium supply. *Global Biogeochemical Cycles*, 32(9), 1294–1311. <https://doi.org/10.1029/2017gb005839>

Hayes, C. T., Fitzsimmons, J. N., Boyle, E. A., McGee, D., Anderson, R. F., Weisend, R., & Morton, P. L. (2015). Thorium isotopes tracing the iron cycle at the Hawaii Ocean Time-series Station ALOHA. *Geochimica et Cosmochimica Acta*, 169, 1–16. <https://doi.org/10.1016/j.gca.2015.07.019>

Ito, A., Myriokefalitakis, S., Kanakidou, M., Mahowald, N. M., Scanza, R. A., Hamilton, D. S., et al. (2019). Pyrogenic iron: The missing link to high iron solubility in aerosols. *Science Advances*, 5(5), eaau7671. <https://doi.org/10.1126/sciadv.aau7671>

Jickells, T. D. (1999). The inputs of dust derived elements to the Sargasso Sea: A synthesis. *Marine Chemistry*, 68(1–2), 5–14. [https://doi.org/10.1016/s0304-4203\(99\)00061-4](https://doi.org/10.1016/s0304-4203(99)00061-4)

Jickells, T. D., An, Z. S., Andersen, K. K., Baker, A. R., Bergametti, G., Brooks, N., et al. (2005). Global iron connections between desert dust, ocean biogeochemistry, and climate. *Science*, 308(5718), 67–71. <https://doi.org/10.1126/science.1105959>

Kadko, D., Aguilar-Islas, A., Bolt, C., Buck, C. S., Fitzsimmons, J. N., Jensen, L. T., et al. (2019). The residence times of trace elements determined in the surface Arctic Ocean during the 2015 US Arctic GEOTRACES expedition. *Marine Chemistry*, 208, 56–69. <https://doi.org/10.1016/j.marchem.2018.10.011>

Kadko, D., Landing, W. M., & Buck, C. S. (2020). Quantifying atmospheric trace element deposition over the ocean on a global scale with satellite rainfall products. *Geophysical Research Letters*, 47(7), e2019GL086357. <https://doi.org/10.1029/2019gl086357>

Kim, G., & Church, T. M. (2001). Seasonal biogeochemical fluxes of  $^{234}\text{Th}$  and  $^{210}\text{Po}$  in the Upper Sargasso Sea: Influence from atmospheric iron deposition. *Global Biogeochemical Cycles*, 15(3), 651–661. <https://doi.org/10.1029/2000gb001313>

Kustka, A., Carpenter, E. J., & Sañudo-Wilhelmy, S. A. (2002). Iron and marine nitrogen fixation: Progress and future directions. *Research in Microbiology*, 153(5), 255–262. [https://doi.org/10.1016/s0923-2508\(02\)01325-6](https://doi.org/10.1016/s0923-2508(02)01325-6)

Lagerström, M. E., Field, M. P., Séguert, M., Fischer, L., Hann, S., & Sherrell, R. M. (2013). Automated on-line flow-injection ICP-MS determination of trace metals (Mn, Fe, Co, Ni, Cu and Zn) in open ocean seawater: Application to the GEOTRACES program. *Marine Chemistry*, 155, 71–80. <https://doi.org/10.1016/j.marchem.2013.06.001>

Lomas, M. W., Bates, N. R., Johnson, R. J., Knap, A. H., Steinberg, D. K., & Carlson, C. A. (2013). Two decades and counting: 24-years of sustained open ocean biogeochemical measurements in the Sargasso Sea. *Deep Sea Research Part II: Topical Studies in Oceanography*, 93, 16–32. <https://doi.org/10.1016/j.dsr2.2013.01.008>

Mahowald, N. M., Hamilton, D. S., Mackey, K. R., Moore, J. K., Baker, A. R., Scanza, R. A., & Zhang, Y. (2018). Aerosol trace metal leaching and impacts on marine microorganisms. *Nature Communications*, 9(1), 2614. <https://doi.org/10.1038/s41467-018-04970-7>

Martin, J. H., Gordon, M., & Fitzwater, S. E. (1991). The case for iron. *Limnology & Oceanography*, 36(8), 1793–1802. <https://doi.org/10.4319/lo.1991.36.8.1793>

Middag, R., Séférian, R., Conway, T. M., John, S. G., Bruland, K. W., & de Baar, H. J. (2015). Intercomparison of dissolved trace elements at the Bermuda Atlantic Time Series station. *Marine Chemistry*, 177, 476–489. <https://doi.org/10.1016/j.marchem.2015.06.014>

Moore, C. M., Mills, M. M., Arrigo, K. R., Berman-Frank, I., Bopp, L., Boyd, P. W., et al. (2013). Processes and patterns of oceanic nutrient limitation. *Nature Geoscience*, 6(9), 701–710. <https://doi.org/10.1038/ngeo1765>

Morton, P. L., Landing, W. M., Hsu, S. C., Milne, A., Aguilar-Islas, A. M., Baker, A. R., et al. (2013). Methods for the sampling and analysis of marine aerosols: Results from the 2008 GEOTRACES aerosol intercalibration experiment. *Limnology and Oceanography: Methods*, 11(2), 62–78. <https://doi.org/10.4319/lom.2013.11.62>

Prospero, J. M., Ginoux, P., Torres, O., Nicholson, S. E., & Gill, T. E. (2002). Environmental characterization of global sources of atmospheric soil dust identified with the Nimbus 7 Total Ozone Mapping Spectrometer (TOMS) absorbing aerosol product. *Reviews of Geophysics*, 40(1), 2–1. <https://doi.org/10.1029/2000rg000095>

Sedwick, P. N., Bowie, A. R., Church, T. M., Cullen, J. T., Johnson, R. J., Lohan, M. C., et al. (2020). Dissolved iron in the Bermuda region of the subtropical North Atlantic Ocean: Seasonal dynamics, mesoscale variability, and physicochemical speciation. *Marine Chemistry*, 219, 103748. <https://doi.org/10.1016/j.marchem.2019.103748>

Sedwick, P. N., Church, T. M., Bowie, A. R., Marsay, C. M., Ussher, S. J., Achilles, K. M., et al. (2005). Iron in the Sargasso Sea (Bermuda Atlantic Time-series Study region) during summer: Eolian imprint, spatiotemporal variability, and ecological implications. *Global Biogeochemical Cycles*, 19(4), GB4006. <https://doi.org/10.1029/2004gb002445>

Sedwick, P. N., Sholkovitz, E. R., & Church, T. M. (2007). Impact of anthropogenic combustion emissions on the fractional solubility of aerosol iron: Evidence from the Sargasso Sea. *Geochemistry, Geophysics, Geosystems*, 8(10), Q10Q06. <https://doi.org/10.1029/2007gc001586>

Sedwick, P. N., Sohst, B. M., O'Hara, C., Stammerjohn, S. E., Loose, B., Dinniman, M. S., et al. (2022). Seasonal dynamics of dissolved iron on the Antarctic continental shelf: Late-fall observations from the Terra Nova Bay and Ross Ice Shelf Polynyas. *Journal of Geophysical Research: Oceans*, 127(10), e2022JC018999. <https://doi.org/10.1029/2022jc018999>

Sedwick, P. N., Sohst, B. M., Ussher, S. J., & Bowie, A. R. (2015). A zonal picture of the water column distribution of dissolved iron (II) during the US GEOTRACES North Atlantic transect cruise (GEOTRACES GA03). *Deep Sea Research Part II: Topical Studies in Oceanography*, 116, 166–175. <https://doi.org/10.1016/j.dsr2.2014.11.004>

Shelley, R. U., Landing, W. M., Ussher, S. J., Planquette, H., & Sarthou, G. (2018). Regional trends in the fractional solubility of Fe and other metals from North Atlantic aerosols (GEOTRACES cruises GA01 and GA03) following a two-stage leach. *Biogeosciences*, 15(8), 2271–2288. <https://doi.org/10.5194/bg-15-2271-2018>

Sholkovitz, E. R., & Sedwick, P. N. (2006). Open-ocean deployment of a buoy-mounted aerosol sampler on the Bermuda Testbed Mooring: Aerosol iron and sea salt over the Sargasso Sea. *Deep Sea Research Part I: Oceanographic Research Papers*, 53(3), 547–560. <https://doi.org/10.1016/j.dsr.2005.12.002>

Sholkovitz, E. R., Sedwick, P. N., Church, T. M., Baker, A. R., & Powell, C. F. (2012). Fractional solubility of aerosol iron: Synthesis of a global-scale data set. *Geochimica et Cosmochimica Acta*, 89, 173–189.

Siegel, D. A., Michaels, A. F., Sorenson, J. C., O'Brien, M. C., & Hammer, M. A. (1995). Seasonal variability of light availability and utilization in the Sargasso Sea. *Journal of Geophysical Research*, 100(C5), 8695–8713. <https://doi.org/10.1029/95jc00447>

Skoog, D. A., Holler, F. J., & Crouch, S. R. (2007). *Principles of instrumental analysis* (6th ed.). Thomson Brooks/Cole.

Sorooshian, A., Corral, A. F., Braun, R. A., Cairns, B., Crosbie, E., Ferrare, R., et al. (2020). Atmospheric research over the western North Atlantic Ocean region and North American East Coast: A review of past work and challenges ahead. *Journal of Geophysical Research: Atmospheres*, 125(6), e2019JD031626. <https://doi.org/10.1029/2019jd031626>

Stafford, R. G., & Ettinger, H. J. (1972). Filter efficiency as a function of particle size and velocity. *Atmospheric Environment*, 6(5), 353–362. [https://doi.org/10.1016/0004-6981\(72\)90201-6](https://doi.org/10.1016/0004-6981(72)90201-6)

Steinberg, D. K., Carlson, C. A., Bates, N. R., Johnson, R. J., Michaels, A. F., & Knap, A. H. (2001). Overview of the US JGOFS Bermuda Atlantic time-series study (BATS): A decade-scale look at ocean biology and biogeochemistry. *Deep Sea Research Part II: Topical Studies in Oceanography*, 48(8–9), 1405–1447. [https://doi.org/10.1016/s0967-0645\(00\)00148-x](https://doi.org/10.1016/s0967-0645(00)00148-x)

Tagliabue, A., Aumont, O., DeAth, R., Dunne, J. P., Dutkiewicz, S., Galbraith, E., et al. (2016). How well do global ocean biogeochemistry models simulate dissolved iron distributions? *Global Biogeochemical Cycles*, 30(2), 149–174. <https://doi.org/10.1002/2015gb005289>

Tagliabue, A., Bowie, A. R., Boyd, P. W., Buck, K. N., Johnson, K. S., & Saito, M. A. (2017). The integral role of iron in ocean biogeochemistry. *Nature*, 543(7643), 51–59. <https://doi.org/10.1038/nature21058>

Tian, Z., Ollivier, P., Veron, A., & Church, T. M. (2008). Atmospheric Fe deposition modes at Bermuda and the adjacent Sargasso Sea. *Geochemistry, Geophysics, Geosystems*, 9(8), Q08007. <https://doi.org/10.1029/2007gc001868>

Tin, H. C., Lomas, M. W., & Ishizaka, J. (2016). Satellite-derived estimates of primary production during the Sargasso Sea winter/spring bloom: Integration of in-situ time-series data and ocean color remote sensing observations. *Regional Studies in Marine Science*, 3, 131–143. <https://doi.org/10.1016/j.rsma.2015.07.002>

Ussher, S. J., Achterberg, E. P., Powell, C., Baker, A. R., Jickells, T. D., Torres, R., & Worsfold, P. J. (2013). Impact of atmospheric deposition on the contrasting iron biogeochemistry of the North and South Atlantic Ocean. *Global Biogeochemical Cycles*, 27(4), 1096–1107. <https://doi.org/10.1002/gbc.20056>

Wen, Z., Browning, T. J., Cai, Y., Dai, R., Zhang, R., Du, C., et al. (2022). Nutrient regulation of biological nitrogen fixation across the tropical western North Pacific. *Science Advances*, 8(5), eabf7564. <https://doi.org/10.1126/sciadv.abf7564>

Wu, J., & Boyle, E. (2002). Iron in the Sargasso Sea: Implications for the processes controlling dissolved Fe distribution in the ocean. *Global Biogeochemical Cycles*, 16(4), 33–1. <https://doi.org/10.1029/2001gb001453>